An experimental system to detect a labeled cell monolayer in a microfluidic environment

Nicolas Gargam, Luc Darrasse, Jean-Sebastien Raynaud, Jean-Christoph Ginefri, Philippe Robert, Marie Poirier-Quinot

An experimental system to detect a labeled cell monolayer in a microfluidic environment

Abbreviated title page: A novel experimental system to detect a labeled cell monolayer in a microfluidic environment

Keywords: MR Contrast Agent, Multi Turn Transmission Line Resonator, microfluidic, cell monolayer

Abbreviations: CA: contrast agent

MTLR : multi-turn transmission-line resonator

ICP-MS : Inductively Coupled Plasma-Mass Spectroscopy

VFA : variable flip angle

Word count: 4742 (include references and legends)

Nicolas Gargam ; Luc Darrasse ; Jean-Sebastien Raynaud ; Jean-Christoph Ginefri ; Philippe Robert ; Marie Poirier-Quinot

ABSTRACT - 223 mots

Introduction - The development of new targeted contrast agents (CA) requires proof-of-concept studies in order to establish the detectability of the CA and to predict the role of biodistribution in its uptake mechanisms. A promising approach is to carefully mimicking the *in vivo* pharmacokinetical context with reduced experimental complexity compare to *in vivo* situations. As a first step towards this objective, this work investigates the feasibility of detecting a living cell monolayer labeled with Gd-DOTA in a microfluidic environment, by micro-MRI in a 2.35T small-animal system.

Materiel and Methods - A dedicated experimental system was built by combining a microfluidic slide and a radiofrequency probe based on a 6 mm diameter multi-turn transmission-line resonator. Adherent KB cells were incubated with different concentrations of Gd. MRI data were acquired at 2.35 T with a 3D Gradient Echo and a resolution of 12.4 µm perpendicularly to the cell layer. The longitudinal relaxation rate R_1 was measured as a function of the amount of Gd internalized by the cells.

Results - R_1 measurements for different Gd concentration per cells were performed using data with an SNR of 100. Relaxation-rate variations ΔR_1 of 0.035s^{-1} were measured. A quenching effect was observed at Gd concentrations above 20fmol/cell.

Conclusion - Our results suggest that this dedicated experimental system is suitable for specifically assessing new high-relaxivity targeted CA under real-time uptake conditions.

INTRODUCTION

In the past decade, a variety of innovative MRI approaches have been proposed to depict molecular processes occurring at cell level, such as the use of exogenous contrast agents (CA). In the context of molecular MRI, the sensitivity to probe molecular markers, in the nanomolar range in most pathological processes, is the critical point (1). The corresponding CA concentration is substantially lower than the detection threshold of gadolinium chelates, which is in the hundred micromolar range (2). Therefore, the detection sensitivity of routinely used gadolinium chelates is inadequate for molecular MR imaging in many cases. To overcome these limitations, CA prototypes, which are able to carry up to several thousand Gd3+ ions, are being developed (3-5). These new particles possess both longer intravascular half-lives and higher longitudinal relaxivities (r_1), so they are good candidates to enable receptor detection in the picomolar range and allow MR imaging of sparse binding sites (6).

In this context, new experimental tools are needed to characterize new molecular contrast agents and evaluate their efficiency. To date, results of *ex vivo* evaluation of most agents are applied directly to *in vivo* animal studies (7). Often, the former relaxation properties of novel CA measured *in vitro* do not correctly reflect the agent's *in vivo* properties (1). Indeed, they do not match the real physiological conditions for the targeting of cellular receptors, in terms receptor concentrations and time of contact between the CA and the receptors; moreover, they are unable to predict the pharmacokinetics of the CA.

Following an intravenous injection of a CA with *in vivo* animal models, many processes can occur simultaneously, such as extravasation, specific binding to receptors, or internalization inside cells. Depending on the process, the CA will have access to different numbers of water molecules and will involve different relaxation pathways (8,9). Thus the relaxation properties of new contrast agents should be initially evaluated and optimized in controlled cell culture studies prior to *in vivo* animal experimentation. Such studies would allow better assessment of the efficiency of the CA as a function of its biodistribution.

This paper investigates the feasibility of detecting a living cell monolayer, labeled with Gd-DOTA (Guerbet Research®), by micro-MRI in a carefully controlled microfluidic environment. The goal of our work was to accurately assess the performance of our experimental system using a conventional Gadolinium labeling technique.

MATERIALS AND METHODS

CA internalization and cell monolayer preparation:

KB cells, a human cell line derived from a nasopharynx carcinoma, were grown in RPMI 1640 medium (Bracco, Italy) supplemented with 10 % Newborn Calf Serum Heat-Inactivated and 1% Glutamine in a humidified incubator at 37 °C and 5 % CO_2. For cell labeling experiments, a protocol inspired by Terreno et al. (8) was used: 2 million cells were seeded inside a 25 cm^2 flask and incubated for 24 hours to make them adhere to the surface of the flask. Following this, cells were put in contact with culture

medium containing Gd-DOTA at concentrations of 0, 1, 2, 5, 10, 25, 50, 75 and 100 mM during 17 h. The Gadolinium content per cell was measured by Inductively Coupled Plasma-Mass Spectroscopy (ICP-MS). 3.50×10^5 labeled cells were seeded into the microfluidic channel coated with Collagen-IV (dimensions of $0.4 \times 5 \times 50\ mm^3$) of a microscope slide (µ-slide I 0.4 Luer, Ibidi, Germany), and formed a confluent single layer as illustrated in Figure 1.c, observed by optical microscopy. The cells were left 4 hours in the microfluidic channel prior to MRI. Preliminary studies of cell viability, using an eosin exclusion test, demonstrated that incubation of the cells during 24 hours with Gd-DOTA concentrations as high as 100 mM in the labeling solution had no toxic effect. Optical microscopy confirmed that 96% of the adherent cells were still alive on the slide after the MRI exam.

Experimental protocol:

The relaxation rates were measured using the variable flip angle (VFA) method (11) with seven flip angles varying from 5 to 70°.

The longitudinal relaxation rate R_1 measurements were first realized in the microfluidic channel filled with 5 different concentrations of Gd-DOTA (0, 50, 100, 250 and 500 µM) diluted in water to assess the VFA method accuracy.

In a second step, $R_1([Gd])$ relaxation rate measurements as a function of incubated Gd were done on labeled cell monolayers in the presence of the CA-free

culture medium. The Gd concentration used for the incubation was of 0, 1, 2, 5, 10, 25, 50, 75 and 100 mM. A washing step was done at the end of the experiment on the cell layer with a flush of 5 mL of 38 $g.L^{-1}$ NaClO in the channel. Optical microscopy confirmed that an NaClO flush killed the whole cell layer immediately and removed the cell lysis from the microfluidic channel. The same imaging protocol was applied on the channel before (with labeled cells) and after the flush (culture medium only), to obtain a reference acquisition with exactly the same position of the slide inside the MRI scanner. R_1 values were determined on the cells, $R_{1,c}([Gd])$, and on the CA-free culture medium, $R_{1,m}$.

The effect of the MR CA is $R_1([Gd]) = R_1([Gd=0]) + r_1 . [Gd]$ with $R_1([0])$ the baseline relaxation rate (free medium or cells), r_1 the CA relaxivity, of 3 $mMol.s^{-1}$ in our study (12).

MRI hardware :

Experiments were carried out on a 2.35 T horizontal scanner (Bruker Biospin, Germany), delivering a maximum gradient intensity of 200 mT/m. The microfluidic channel was manually aligned with the static magnetic field to minimize susceptibility artifacts. The quality of the alignment was then monitored by a scout scan. Warm air flowed in the gradient bore to maintain the temperature of the cells at 37 °C. To ensure a homogeneous excitation of the hydrogen nuclei, a birdcage coil (Bruker, Germany) with an inner diameter of 7 cm was used for transmission. The reception coil was a high sensitivity home-made surface coil of 6 mm mean diameter, using the MTLR

design and microfabrication process (13). It was composed of 10 circular concentric copper tracks deposited of both sides of a sapphire substrate. The MTLR was placed below the µ-slide, 180 µm away from the cell monolayer (Figure 1 a. b.) and was inductively coupled (14) to the receiver electronics using a 6 mm single-turn copper loop, parallel tuned at $f_0 = 100.53$ MHz. Orthogonality between the transmit and receive coils axis leaded to a attenuated transmission coefficient S_{21} between the two coils of about – 40 dB at the Larmor frequency.

MRI sequence: A T_1-weighted 3D-FLASH (Fast Low Angle SHot) sequence was used with a field of view of $0.6 \times 1.9 \times 0.8$ cm^3, a resolution of 12.4 µm in the readout direction, perpendicular to the cell layer, and an in-plane resolution of 160×160 μm^2. To reach such high resolution in the readout direction, echo asymmetry was adjusted to 5%, meaning that only 55% of the k-space was acquired. Acquisition parameters were: TR (Time Repetition)/TE (Time Echo) of 74.7/3.7 ms, total sampling bandwidth of 12.5 kHz, 2 averages, 100 dummy scans to reach the steady state, and acquisition time of 8 min. Radiofrequency spoiling was performed with a 117° phase increment between successive excitations to reduce residual transverse magnetization effects. The alignment of the microfluidic channel onto the horizontal image axis was carefully adjusted using scout scans at the beginning of the protocol.

Data Processing

A cylindrical region of interest (ROI) of 5 mm diameter was centered to the sensitivity pattern of the reception coil. One-dimensional signal profiles were then

extracted with a projection signal intensity of the ROI along the 2 directions, y and z, parallel to the cell layer (5 and 50 mm). The homodyne method (15) was applied to ensure low distortion of the reconstructed profiles despite the highly asymmetric k-space coverage. To avoid truncation artifacts, a linear phase ramp correction was applied to the k-space with the appropriate sub-voxel shift before the homodyne reconstruction. The R_1 measurements were performed on the first non-zero voxel along the x-axis, assuming this to be the voxel containing the cells.

The signal-to-noise (SNR) measurements were extracted from magnitude images using the average signal intensity over the ROI and the standard deviation outside of the channel.

The systematic evaluation of the performance of the R_1 measurements was based on Cramer-Rao Bound according to the SNR and the flip angle of the experiments (16).

The relaxation rate was also simulated considering the theoretical model developed by Strijkers et al. (17), based on the Bloch equations including exchanges of water molecules among 3 different compartments (vesicles, cytoplasm and the extracellular medium). Their model allows the quantification of the decreased efficiency due to the CA internalization, depending on the location of the paramagnetic chelates. The shape of the cells highly influences the values of the water molecule exchange constants between two compartments. In the present study, cells are adherent on a surface and were assumed an oblate semi-spheroid cell shape, following

a previous work by Lee et al. (18). This modified model was applied using the parameters of Table 1 to simulate $R_{1,c}$ ([Gd]) measurements, assuming equal relaxation rates between the vesicle, cytosol, and extracellular compartments in the absence of CA. The number of vesicles, their radii, and their permeability were of the same order as those reported in the literature (19-21).

Diffusion

Based on the integration of the Bloch-Torrey equation, this system could be represented by a mean local relaxation time assuming a mono-exponential position-dependent decay (Mean Relaxation Time Approximation (22)). Due to the planar configuration of the cell monolayer (over y and z axes), the apparent relaxation rate $R_{1,local}(x)$, induced by the paramagnetic CA, is expected to vary along the *x*-direction. Considering a time integration of the Bloch-Torrey equation, from 0 to infinity, taking the bulk culture medium's relaxation rate R_{1m}, diffusion coefficient D_m, and assuming the cell monolayer was entirely contained in the first voxel, the local relaxation rate is then expected to vary as :

$$\boldsymbol{R_{1,local}(x)^{-1} = {R_{1,m}}^{-1} + \left({R_{1,local}(0)^{-1} - {R_{1,m}}^{-1}}\right) e^{-\frac{x}{\sqrt{D_m . {R_{1,m}}^{-1}}}}} \quad \textbf{Eq. 1.}$$

Considering a Spoiled Gradient Recalled Echo sequence, with TR = 75 ms, R_{1c} $(x=0)$ and R_{1m} and respectively equal to the cells' relaxation rate and the medium relaxation rate measured on MR acquisitions, $S_{1D,c}$ and $S_{1D,m}$, signals produced for

relaxation rate $R_{1local}(x)$ and R_{1m} were calculated. The theoretical normalized difference, $(S_{1D,c}(x)-S_{1D,m})/S_{1D,m}$ was evaluated.

RESULTS

Figure 2 displays the linear dependence with a slope of 0.499 between the amount of internalized Gd^{3+} per cell and the Gd-DOTA incubation concentration, as measured by ICP-MS.

R_1 measurements on the slide filled with water containing different CA concentrations are shown Figure 3-a (dots); $R_1([Gd])$ were measured on data not shown here with an SNR of about 100. Water CA free relaxation rate, $R_1([0])$ was of 0.38 ± 0.06 s^{-1}. Error bars were estimated from the Cramer Rao Lower Band, an SNR of 100 and R_1 of water of 38 s^{-1}. The theoretical curve was computed considering a Gd-Dota relaxivity of 3 $mM^{-1}.s^{-1}$ (black line). The extrapolation of the relaxation rate of the water CA free was 0.347 ± 0.07 s^{-1}.

Figure 3-b shows the $R_{1,c}([Gd])$ values, R_1 measurements for different Gd concentration, as a function of the Gd content per cell. The measurements were made using data with an SNR of 100. The $R_{1,c}([0])$ was measured at about 0.38 ± 0.13 s^{-1}. The error bars are computed, following the Cramer Rao Lower Band and an SNR of 100 ~~40~~ and $R_{1,c}([0])$ = 0.38. A saturation effect at high Gd content, up to 20 fmol/cell, was also

observed and may be attributed to compartment effect as discussed in the last section. The relaxation rate of the cell-free medium, R_{1m}, was measured as 0.37 ± 0.08 on the slide filled with medium. The black curve in figure 3.b showes the simulated $R_{1,c}$ ([Gd]), based on the Strijkers model.

Figure 4.a presents the signal variation along the x-axis, i.e., the receiver coil axis. The black curve depicts the one-dimensional profile, $S_{1D,m}$, of the CA free medium. The Signal-to-Noise Ratio of the profile was about 100 ~~40~~. The decrease of the signal, by less than 20 % along the coil axis, is due to the B_1 reception field amplitude decay. This curve was used as the reference to evaluate the effect of the labeled cells. The gray curve, $S_{1D,c}$, displays the one-dimensional profile obtained for a channel containing cells after 17 h incubation with 25 mM of Gd-DOTA, corresponding to a Gd content of 15 fmol per cell, and a 20° flip angle. This profile is typically obtained with other Gd concentrations. The adherent cells are confined within the first voxel (x=0) of the microfluidic channel, corresponding to the first maximum of signal of the 1D profile. The signal enhancement was observed both at the level of the labeled cell layer and on adjacent voxels up to a distance of about 150 µm, until $S_{1D,c}$-$S_{1,Dm}$ was equal to the noise level.

The effect of diffusion is analysed on Figure 4.b. The black points represent the measured normalized difference, $\frac{S_{1D,c}-S_{1D,m}}{S_{1D,m}}$, obtained from the experiments. The theoretical normalized difference, black line, is fitted to the experimental data considering that D_m equals 2.8 10^9 $m^2.s^{-1}$ and $R_{1,m}$ is 0.37 s^{-1}. A $R_{1,local}$ (x=0) of 0.62 ± 0.017 s^{-1} was then obtained.

DISCUSSION

In this study, we propose an experimental system to detect and measure the relaxation rate of a single cell layer by micro-MRI, a very difficult challenge given the resolution capabilities at clinical. This initial study was carried out using KB cells treated with independently determined concentrations of Gd-DOTA. The feasibility and accuracy of R_1 measurements in cell cultures using an MTLR resonator was assessed and confirmed with aqueous Gd-DOTA samples of known concentration. The high sensitivity of this experimental system is due to the small diameter of the receiver coil. The high spatial resolution then reached for cell detection highlighted the diffusion of R_1 modified water protons through the cell membranes into the culture medium. A transition zone between two compartments with two different R_1 values was observable in the signal profile. A comparable effect has already been observed and investigated by Kaufman et al. (23) with T_1-weighted high-resolution images. Thanks to the planar geometry (slice), all cells are subjected to the same conditions, which will be helpful to dissociate the several compartments involved in the theoretical model developed; here there are two compartments, the cell layer and the culture medium. A theoretical approach by Bauer et al. (24) showed that the effect of a Blood-Pool CA confined to the intravascular space was also observed in the tissue surrounding the capillaries, by transport of the water molecules through the capillary wall and diffusion throughout the extravascular space. Based on the Bloch-Torrey equation (25), they demonstrated that this system could be represented by a mean local relaxation time assuming a mono-exponential position-dependent decay (Mean Relaxation Time

Approximation (22)). In the present case, the paramagnetic CA induced such relaxation behavior in the direction orthogonal to the cell layer. This approach was in good agreement with the experimental measurements. The sensitivity of this system also allowed measurement of a detection limit ΔR_1 of 0.035 s^{-1}, considering the almost linear behavior of R_1 as a function of Gd concentration, for Gd content less than 4 fmol per cell, and a SNR of 100. This corresponds to a variation of the amount of Gd of less than 1 fmol per cell. The saturation of the $R_{1,c}$ curve for Gd contents above 20 fmol [Gd] per cell is well described by a relaxivity quenching effect attributed to the CA internalization in cells via pinocytosis, a non-specific endocytosis process. This phenomenon leads to the entrapment of the CA inside vesicles within the cytoplasm, resulting in decreased CA efficiency (i.e., apparent relaxivity) compared to that of free CA (8). In this study, all $R_{1,c}([Gd])$ values were smaller than 1 s^{-1}, which is low compared to literature values, which are in the 1.5 to 3 s^{-1} range (8,19) for cell pellets that have internalized high amounts of Gadolinium. This difference can be explained by the shape of the cells, which are considered in the literature as spherical in cell pellets; however, in our experiments, cells are adherent and are assumed to be semi-spheroids. When we applied the Strijkers model (17) assuming spherical cells occupying half of a voxel volume, we found R_{1c} values of 2 s^{-1} for high Gd cell contents, which is in agreement with the literature data. The voxel dimension along the x-axis is small enough to be in the right range for the Strijkers model.

Cells occupied more than half of the voxel height. Since the voxels are composed of cells and water, considering the fast exchange limit, R_1 of the water and

R_1 of the cells will contribute to the R_1 measurement in the first voxel. The R_1 measurement of the cells will then probably be overestimated. This could explain the difference between the $R_{1c}([25\mathrm{mM}])$ value measured using the VFA method and the value extrapolated from the Bloch Torrey model at x=0. Moreover, the assumption of a perfectly known value for the angle calibration could be a source of error not considered here. Nevertheless, R_1 measurements of water, medium, and CA-free cells, and those extrapolated from the first experiment were consistent. Moreover, the VFA technics remained robust to the inhomogeneous reception field B_1 considering our experimental configuration, and the short acquisition time of 8 minutes allowed by this technique remains an obvious asset, especially for dynamic experiments. Another limitation of this study may be the small diameter of the receiver coil, which was limited here to values below 6 mm in order to match the microfluidic channel width. Decreasing the coil diameter further would result in a lower integrated signal-to-noise ratio on the 1D profile. Indeed, the coil sensitivity is expected to scale as the inverse of the coil diameter (26), while the number of detected cells in the monolayer would scale as the squared inverse of the diameter. However, combining several smaller coils to form a surface coil array with the same overall dimension as here still offers the perspective of greatly enhancing the detection level.

In conclusion, this experimental system appears suitable for monitoring the dynamic uptake of targeted contrast agents in realistically mimicked *in vivo* conditions. It should allow to predict the CA kinetics to assess the relevant time for imaging. A quite similar approach was proposed by Schmalbrock et al. (10) on cell culture plates, but their

configuration was not practical for assessment of the CA dynamic uptake in a realistic and controlled environment. Here, we propose a promising approach to carefully evaluate the dynamic uptake of contrast agents by cells using *in vitro* models, in order to mimic the *in vivo* pharmacokinetic context with reduced experimental complexity..

REFERENCES

1. Massoud TF, Gambhir SS. Molecular imaging in living subjects: seeing fundamental biological processes in a new light. Genes Dev 2003;17(5):545-580.
2. Schabel MC, Parker DL. Uncertainty and bias in contrast concentration measurements using spoiled gradient echo pulse sequences. Physics in Medicine and Biology 2008;53(9).
3. Swanson SD, Kukowska-Latallo JF, Patri AK, et al. Targeted gadolinium-loaded dendrimer nanoparticles for tumor-specific magnetic resonance contrast enhancement. Int J Nanomedicine 2008;3(2):201-210.
4. Mulder WJ, Strijkers GJ, van Tilborg GA, Griffioen AW, Nicolay K. Lipid-based nanoparticles for contrast-enhanced MRI and molecular imaging. NMR Biomed 2006;19(1):142-164.
5. Ghaghada KB, Ravoori M, Sabapathy D, Bankson J, Kundra V, Annapragada A. New dual mode gadolinium nanoparticle contrast agent for magnetic resonance imaging. PLoS One 2009;4(10):e7628.
6. Morawski AM, Winter PM, Crowder KC, et al. Targeted nanoparticles for quantitative imaging of sparse molecular epitopes with MRI. Magnetic resonance in medicine : official journal of the Society of Magnetic Resonance in Medicine / Society of Magnetic Resonance in Medicine 2004;51(3):480-486.
7. Mishra R, Su W, Pohmann R, et al. Cell-penetrating peptides and peptide nucleic acid-coupled MRI contrast agents: evaluation of cellular delivery and target binding. Bioconjugate chemistry 2009;20(10):1860-1868.
8. Terreno E, Geninatti Crich S, Belfiore S, et al. Effect of the intracellular localization of a Gd-based imaging probe on the relaxation enhancement of water protons. Magnetic Resonance in Medicine: Official Journal of the Society of Magnetic Resonance in Medicine / Society of Magnetic Resonance in Medicine 2006;55(3):491-497.
9. Kok MB, Hak S, Mulder WJ, van der Schaft DW, Strijkers GJ, Nicolay K. Cellular compartmentalization of internalized paramagnetic liposomes strongly influences both T1 and T2 relaxivity. Magnetic resonance in medicine : official journal of the Society of Magnetic Resonance in Medicine / Society of Magnetic Resonance in Medicine 2009;61(5):1022-1032.
10. Schmalbrock P, Hines JV, Lee SM, Ammar GM, Kwok EWC. T1 measurements in cell cultures: A new tool for characterizing contrast agents at 1.5T. Journal of Magnetic Resonance Imaging 2001;14(5):636-648.
11. Fram E, Herfkens R, Johnson, et al. Rapid calculation of T1 using variable flip angle gradient refocused imaging. Magnetic Resonance Imaging 1987;5(3):201-208.
12. Rohrer M, Bauer H, Mintorovitch J, Requardt M, Weinmann HJ. Comparison of magnetic properties of MRI contrast media solutions at different magnetic field strengths. Invest Radiol 2005;40(11):715-724.
13. Serfaty S, Haziza N, Darrasse L, Kan S. Multi-turn split-conductor transmission-line resonators. Magnetic resonance in medicine : official journal of the Society of Magnetic Resonance in Medicine / Society of Magnetic Resonance in Medicine 1997;38(4):687-689.
14. Decorps M, Blondet P, Reutenauer H, Albrand JP, Remy C. An Inductively Coupled, Series-Tuned NMR Probe. J Magn Reson 1985;65(1):100-109.
15. Noll DC, Nishimura DG, Macovski A. Homodyne detection in magnetic resonance imaging. IEEE Trans Med Imaging 1991;10(2):154-163.

16. Rao CR. Information and accuracy attainable in the estimation of statistical parameters. Bulletin of the Calcutta Mathematical Society 1945;37(3):81-91.
17. Strijkers GJ, Hak S, Kok MB, Springer Jr CS, Nicolay K. Three compartment T1 relaxation model for intracellular paramagnetic contrast agents. Magnetic Resonance in Medicine 2009;61(5):1049-1058.
18. Lee DW, Kang IS. Minimum drag shape of a semi-ellipsoid exposed to shear flow and its possible relation to the shape of endothelial cell. Mathematical Biosciences 2011;231(2):225-234.
19. Gianolio E, Arena F, Strijkers GJ, Nicolay K, Högset A, Aime S. Photochemical activation of endosomal escape of MRI-Gd-agents in tumor cells. Magnetic Resonance in Medicine: Official Journal of the Society of Magnetic Resonance in Medicine / Society of Magnetic Resonance in Medicine 2011;65(1):212-219.
20. Wilhelm C, Billotey C, Roger J, Pons JN, Bacri JC, Gazeau F. Intracellular uptake of anionic superparamagnetic nanoparticles as a function of their surface coating. Biomaterials 2003;24(6):1001-1011.
21. Zhao L, Kroenke CD, Song J, Piwnica-Worms D, Ackerman JJH, Neil JJ. Intracellular water-specific MR of microbead-adherent cells: the HeLa cell intracellular water exchange lifetime. NMR in Biomedicine 2008;21(2):159-164.
22. Nadler W, Schulten K. Generalized Moment Expansion for Brownian Relaxation Processes. Journal of Chemical Physics 1985;82(1):151-160.
23. Kaufmann I, Seiberlich N, Haase A, Jakob P. Diffusion generated T1 and T2 contrast. J Magn Reson 2008;192(1):139-150.
24. Bauer WR, Schulten K. Theory of contrast agents in magnetic resonance imaging: coupling of spin relaxation and transport. Magnetic resonance in medicine : official journal of the Society of Magnetic Resonance in Medicine / Society of Magnetic Resonance in Medicine 1992;26(1):16-39.
25. Torrey HC. Bloch Equations with Diffusion Terms. Physical Review 1957;104(3):563-565.
26. Hoult DI, Richards RE. The signal-to-noise ratio of the nuclear magnetic resonance experiment. J Magn Reson 1976;24:71-85.

Legends

Figure 1: Description and dimensions of the complete experimental system: a. photographe of the microscope slide (µ-slide) containing a microfluidic channel in situ with MTLR placed below the µ-slide, 180 µm away from the cell monolayer. Cells adherent and forming a compact monolayer are observable on the bottom in the µfluidic channel (in orange). b - Dimensions and spatial image parameters (field of view, spatial resolution) of the microscope slice. x-axis, orthogonal to the cell monolayer is well highlighted. c - Confluent single layer observed by optical microscopy.

Figure 2: Amount of internalized Gd^{3+} per cell (fmol/cell), measured by ICP-MS, as a function of the Gd-DOTA incubation concentration (black dots). Gd^{3+} per cell evolved linearly (slope of 0.4996) with the Gd-DOTA incubation concentration (black line).

Figure 3: a- R_1 measurements as a function of the Gd-DOTA concentration. The microfluidic channel was filled with an aqueous solution of Gd-DOTA (circle). R_1 theoretical values (black curve) adjusted to experimental values, considering an r_1 of 3 $mM^{-1}.s^{-1}$ at 2.35 T. Error bars were computed from the Cramer Rao lower bound, with an SNR of 100 and $R_{1,c}([0])$ of 0.38. b – longitudinal relaxation rate R_1 of cells ($R_{1,c}$) as a function of the Gd content per cell (fmol/cell) (circle). Error bars were computed from

the Cramer Rao lower bound, with an SNR of 40 and $R_{1,c}([0]) = 0.38$. Black curve represented the R_1 adjustment using the 3-compartment Strijkers model.

Figure 4: a- 1D monocellular layer profile after Gd-DOTA incubation (25 mM) corresponding to 15 fmol/cell, $S_{1D,c}$, was represented on the gray curve. 1D medium profile without cell, $S_{1D,m}$, is represented on the black one. Both were obtained with the same sequence parameters and a flip angle of 20°. The decrease of 20 % of the signal along the coil axis on the red curve was attributed to the B_1 field of the reception coil. (1), (2), (3) and (4) are relative to spatial position located on the experimental system (Figure 1) b -The normalized difference, $\frac{S_{1D,c}-S_{1D,m}}{S_{1D,m}}$, black points, describes the variations of the signal as a function of the distance from the cell monolayer. The theoretical normalized difference is adjusted to the experimental data (line curve) assuming the Bloch Torrey diffusion model, considering a SPGR sequence, with TR = 75 ms, $R_{1,m} = 0.37\ s^{-1}$ and $D_m = 2.8 \times 10^9\ m^2.s^{-1}$. The $R_{1,app}(x=0)$ value of 0.62 ± 0.017 s^{-1} is obtained.

Table 1 : Parameters used for simulation of $R_{1,c}$([Gd]) expected (represent by the gray curve on figure 3.b) considering the 3-compartment Strijkers model (20).

Table 1

Gd-DOTA longitudinal relaxivity r_1 ($mM^{-1}.s^{-1}$)	3
Cell basis radius (μm)	19
Cell height (μm)	7
Water Membrane permeability ($\mu m.s^{-1}$)	20
Number of vesicles	25
Vesicle radius (μm)	1
Extracellular water fraction	0.7
Culture medium relaxation rate (s^{-1})	0.38
Cytosol relaxation rate (s^{-1})	0.38
Vesicle relaxation rate (s^{-1})	0.38

a.

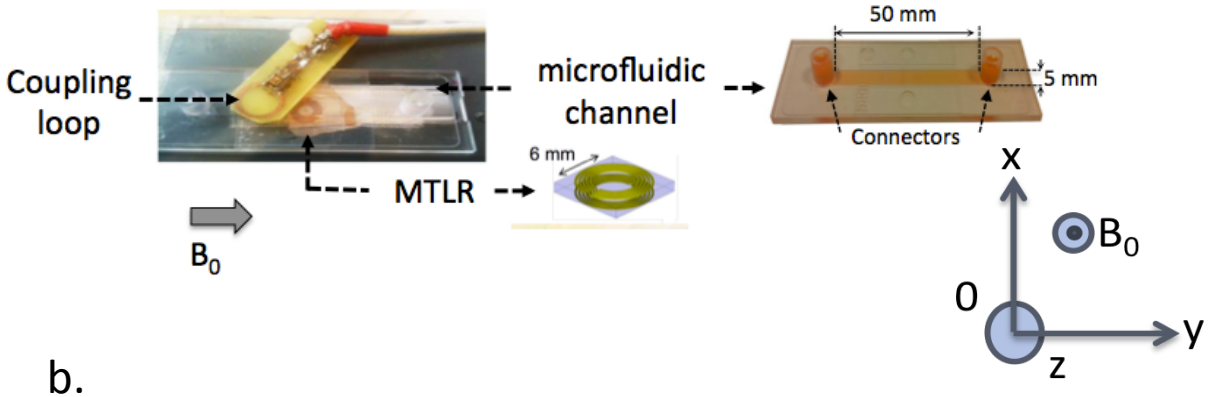
Coupling loop
microfluidic channel
50 mm
5 mm
Connectors
6 mm
MTLR
B0
x
B0
0
y
z

b.

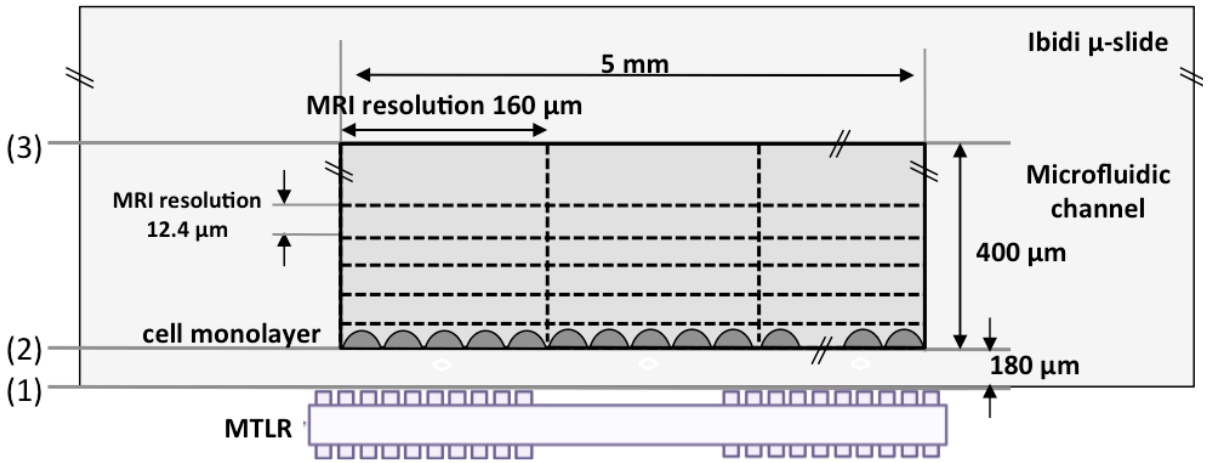
Ibidi µ-slide
5 mm
MRI resolution 160 µm
(3)
MRI resolution 12.4 µm
Microfluidic channel
400 µm
cell monolayer
(2)
180 µm
(1)
MTLR

c.

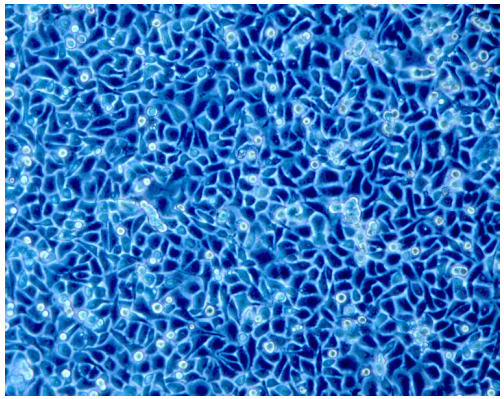

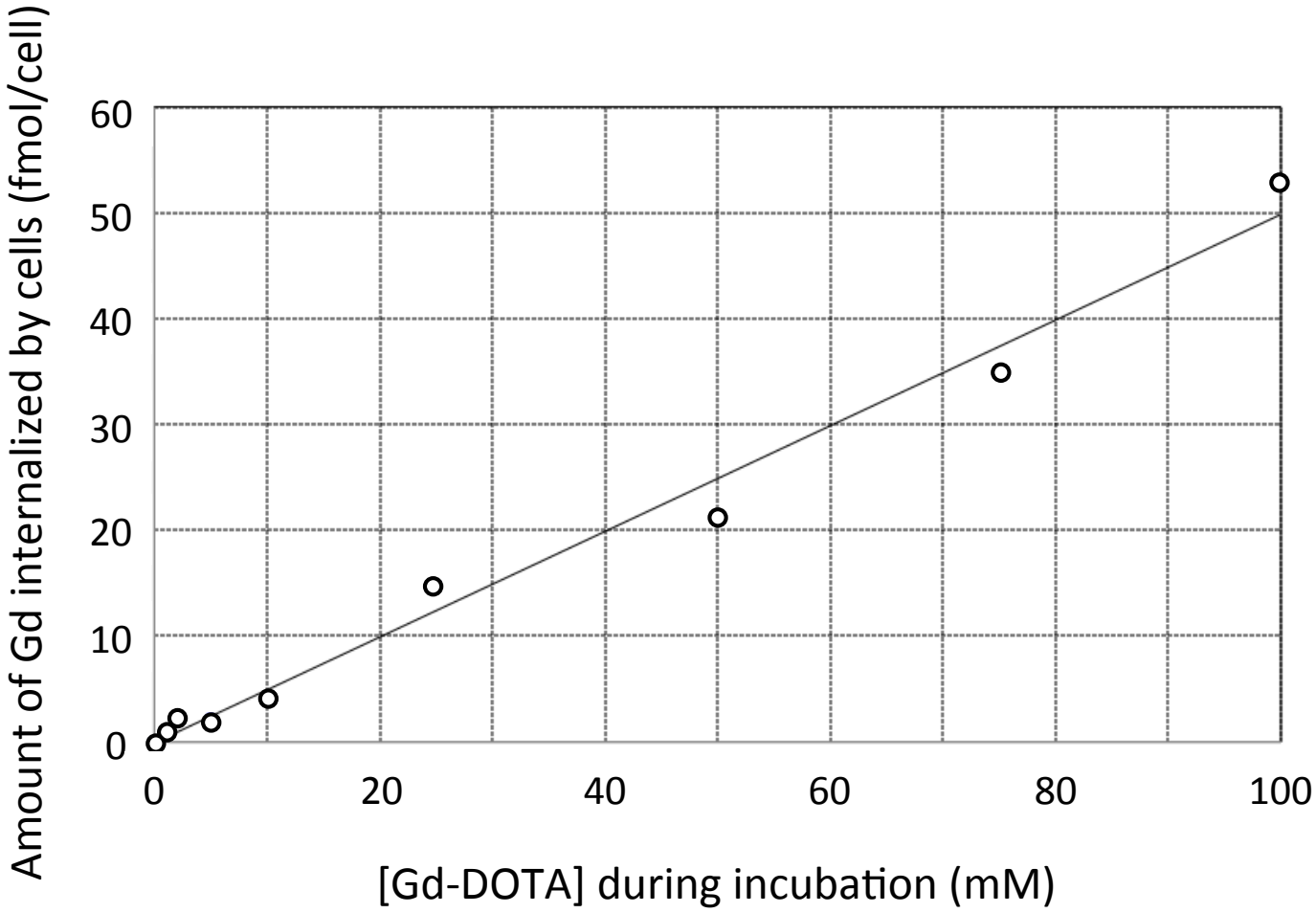
Amount of Gd internalized by cells (fmol/cell)
60
50
40
30
20
10
0
0
20
40
60
80
100
[Gd-DOTA] during incubation (mM)

a.

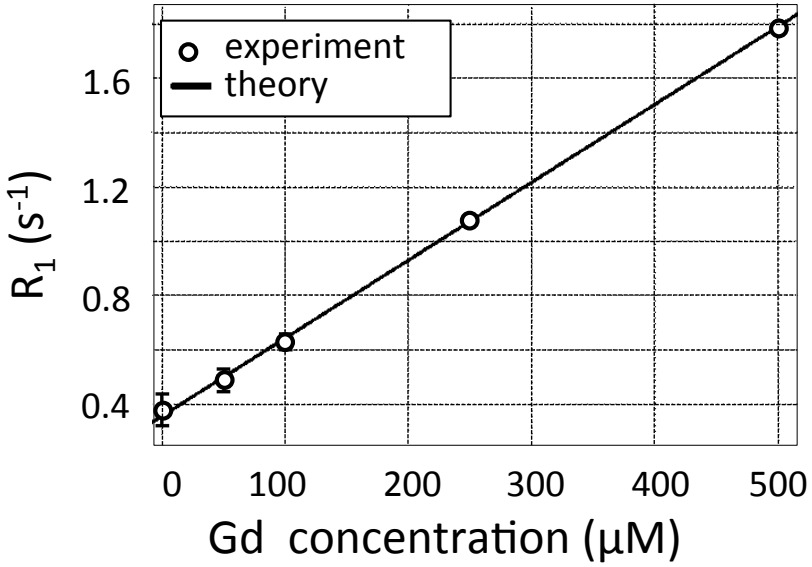
experiment
theory
1.6
1.2
0.8
0.4
R_1 (s^{-1})
0
100
200
300
400
500
Gd concentration (μM)

b.

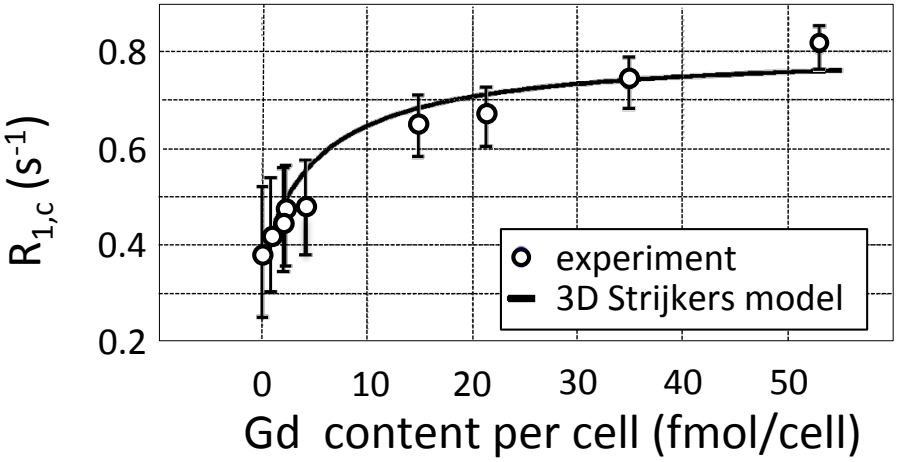
0.8
0.6
0.4
0.2
$R_{1,c}$ (s^{-1})
experiment
3D Strijkers model
0
10
20
30
40
50
Gd content per cell (fmol/cell)

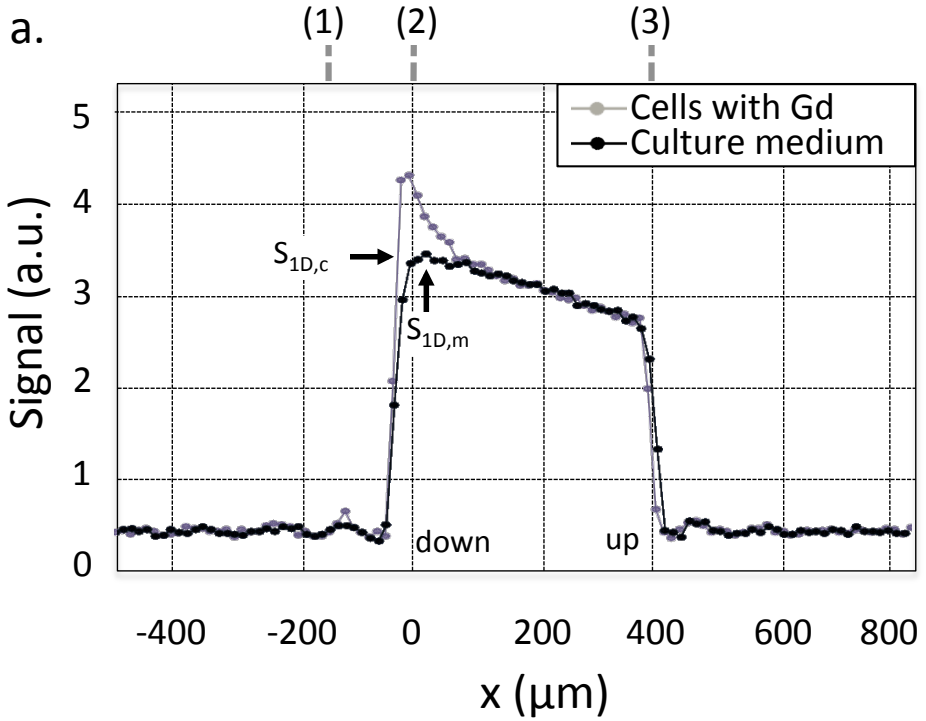
a.
(1)
(2)
(3)
Cells with Gd
Culture medium
Signal (a.u.)
$S_{1D,c}$
$S_{1D,m}$
down
up
x (µm)

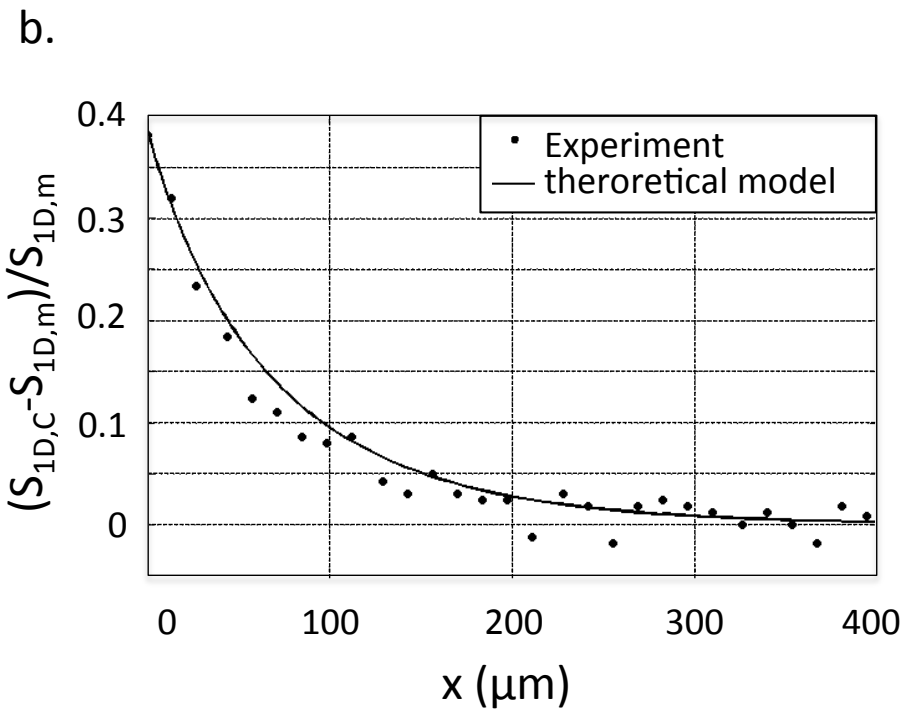
b.
Experiment
theroretical model
$(S_{1D,C}-S_{1D,m})/S_{1D,m}$
x (µm)